Demonstration of a temperature boosting system in district heating

Pierre JC Vogler-Finck, Morten Veis Donnerup (Neogrid Technologies ApS),
Rakesh Sinha, Pavani Ponnaganti, Birgitte Bak Jensen, Jakob Hærvig (Aalborg University)

Neogrid Technologies ApS

Niels Jernes Vej 10
DK-9220 Aalborg Øst
Denmark

info@neogrid.dk
www.neogrid.dk

Table of Content

1 Introduction

The SmartCE2H project includes 2 demonstrators where heat is provided in an innovative way to Danish households. This deliverable focuses on the district heating centred demonstration in the municipality of Skive on a street called Citronvej. Citronvej is located on the outskirt of Skive, where a subpart of it is a dead-end street with 20 single-family houses whose heat is supplied by district heating.

Originally, the plan was to install the heat-pump in a remote area supplied by a low temperature transmission line. However, the local district heating operator did not identify any suitable candidate for such a setup, and proposed instead to simulate this by coupling an area in the vicinity of the city to a return line whose flow temperature would match a low temperature supply line.

Suntherm and Neogrid have designed a booster heat-pump setup to supply district heating to the 20 houses on Citronvej, as well as demonstrated an intelligent controller of the installation in the broader context of the local electricity system.

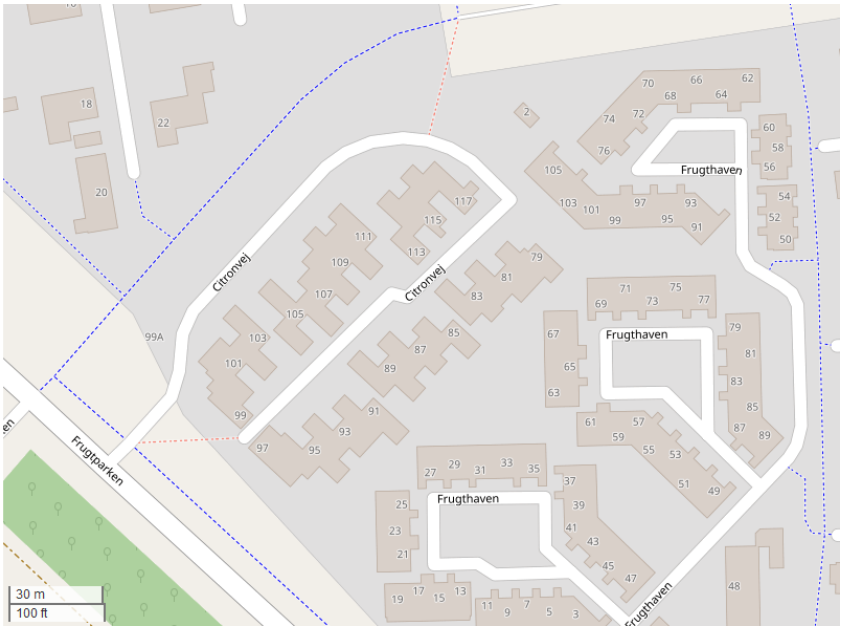

Figure 1: Map of the Citronvej street and its 20 houses in Skive (from OpenStreetMap.org)

The system was demonstrated in the winter 2021-2022. The demonstration should have continued running until 2023, which has not been possible due to a technical issue with a flow switch on the heat-pump and a change in flow conditions on the return line which prevented its further usage as a heat source. Therefore, the figures presented in the rest of the report cover the period up to spring 2022.

This deliverable introduces the structure of the booster station, experiments carried out during the first year of its operation, as well as learnings derived from this demonstration.

2 Overview of the technical installation

This section presents the technical installation of the booster heat-pump.

2.1 Dimensioning of the system

In a first step, Neogrid has carried out an estimation of the heat demand of the area, based upon meter data from the houses which have been provided by the local district heating operator (Skive Fjernvarme). This estimation was based upon consumption readings with daily resolution, which were coupled together with historical data for the area.

The dimensioning has been based upon aggregation of the 20 houses, whose demand profiles (power and flow, as well as average supply temperature at daily level) are plotted below.

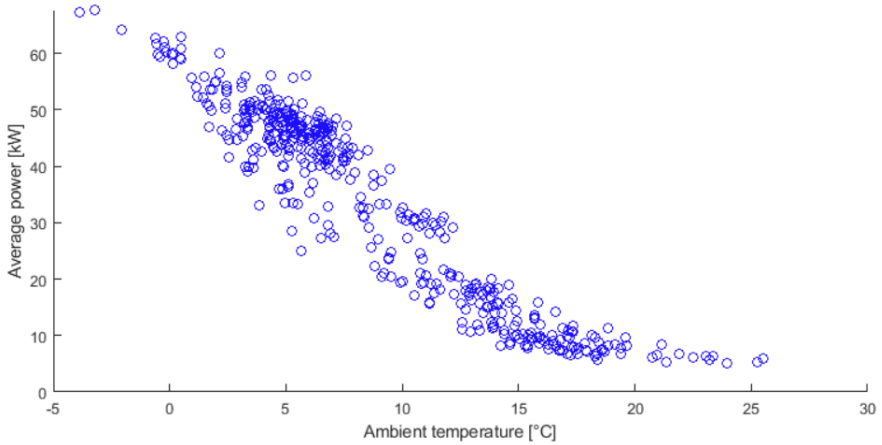

Figure 2: Average power demand profile of the sum of the households (using a daily average and historical data)

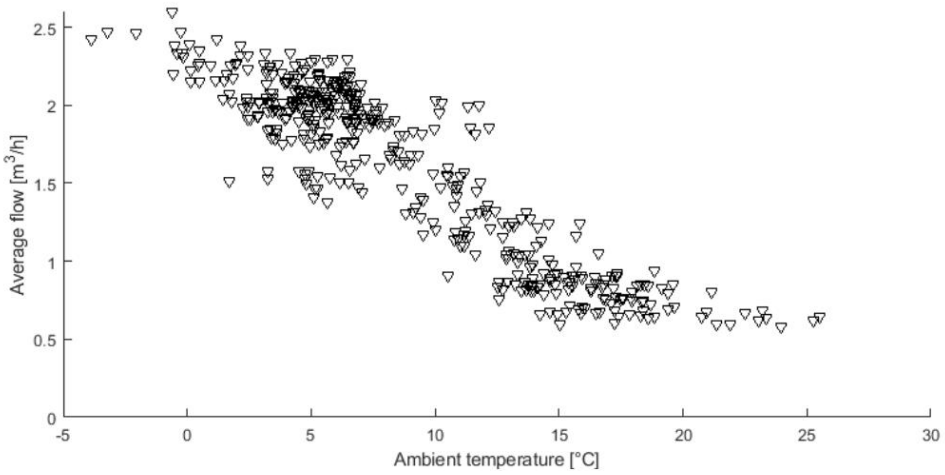

Figure 3: Average flow demand profile of the sum of the households (using a daily average and historical data)

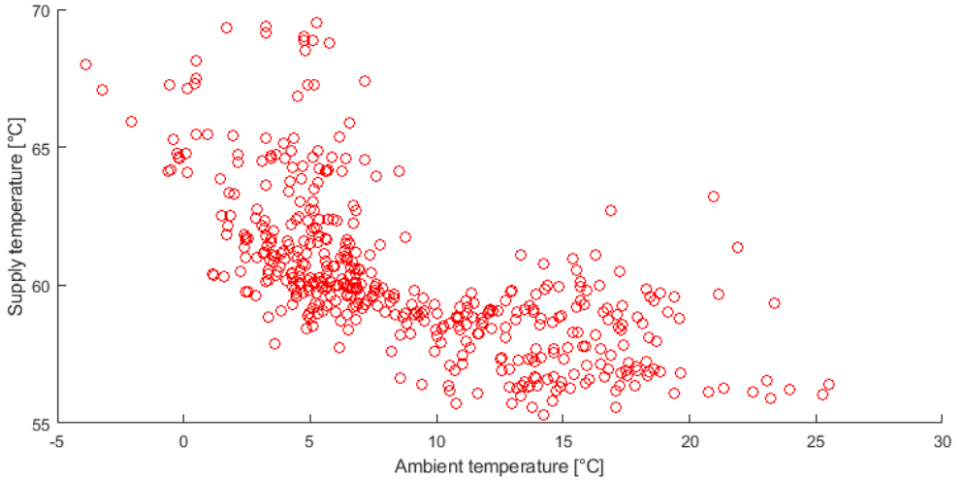

Figure 4: Supply temperature profile of the sum of the households (using a daily average and historical data)

This analysis provided an order of magnitude for the required dimensioning of the installation, with maximum daily averages of power and flow of about 70 kW and 2.6 m^3/h respectively, as well as a supply temperature fluctuating between 55 and 70°C.

Given that these figures reflect the demand side with a daily resolution, an operational margin was required to account for network losses and the fact that the instantaneous demand can at times be considerably higher than the daily average.

2.2 Structure of the system

Based upon the estimates presented above, Suntherm carried out the heat-pump design. The main decision factor was the estimated sum of maximum daily heat load (close to 70 kW), to which a 30% margin was added to account for losses and intra-day variations.

A heat-pump from the manufacturer AERMEC was selected by Suntherm, with characteristics presented in the table below.

Table 1: Characteristics of the booster heat-pump

Manufacturer	AERMEC
Model	WWB0350XHL
Rated electrical power	21.2 kW
Rated heat output	93.1 kW
Number of independent compressors	2 (allowing operation at 0, 50 and 100% of capacity)

The booster station was designed to include a buffer tank on the primary side, to accommodate fluctuations of the flow and its temperature on the primary side, thereby avoiding critical disturbances to the heat-pump operation. On the secondary side, a 3 m^3 storage tank with PCM material was added to provide a buffer for the production allowing to cope with sudden changes in the demand as well as flexibility of the energy production. The melting point of this PCM material was chosen to be 58°C as a compromise between the temperature required to supply the area and cost (components with a higher melting point were considerably more expensive).

A heat exchanger was included on the primary side for pressure management reasons, while another one was added between the PCM storage tank and the local area in order to mitigate the risk of polluting district heating water with PCM material in case of an incident with those components (leakages from the PCM casing had been observed in previous demonstrations on smaller scale systems in rare cases).

The resulting design is presented in the diagram below:

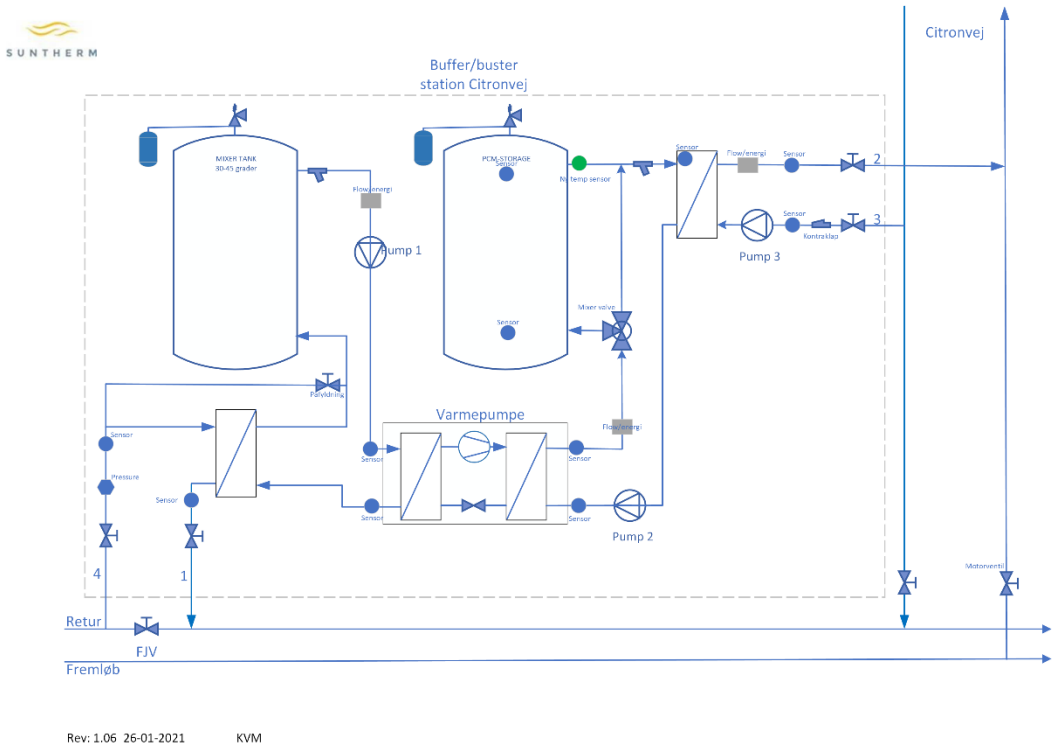

Figure 5: installation diagram of the booster station

The setup included a number of additional sensors allowing detailed monitoring of the installation. One flow/energy meter on the primary side of the heat-pump, another one on the secondary side of the heat-pump, a third one measuring the flow/energy delivered to the street as well as a dedicated electricity meter for the heat-pump. Temperature sensors were later added on the inlet and outlet of the PCM tank in order to be able to assess its state of charge.

For safety purposes, a series of measures were taken:

- a flow switch was included on the heat-pump to ensure that it would not be running without fluid flow (which would result in freezing or overheating)
- thermal expansion tanks (see Figure 7) were added to accommodate changes in the pressure and volume following temperature changes in the installation (this was especially important for the PCM tank which was coupled to 3 of them, as the PCM varies significantly in volume when changing phase)

Figure 6: the booster heat-pump (right) together with the tanks (primary side buffer in the background, PCM in the foreground) installed on Citronvej

Figure 7: thermal expansion tanks for the installation (3 for the PCM tank and one for the buffer tank on the primary side)

To ensure security of supply to the area, the system was designed in a way that allows decoupling of the booster heat-pump and reconnection to the main grid via operation of a valve in a well outside the booster station.

2.3 Characterisation of the booster performance

The performance of the booster heat-pump was characterised in operation, by adjusting the operational conditions over a longer period.

As expected and illustrated on Figure 8, the COP of the heat-pump has a pronounced dependency to the supply temperature, as the source and supply temperature are relatively close (30-40°C and 50-70°C respectively).

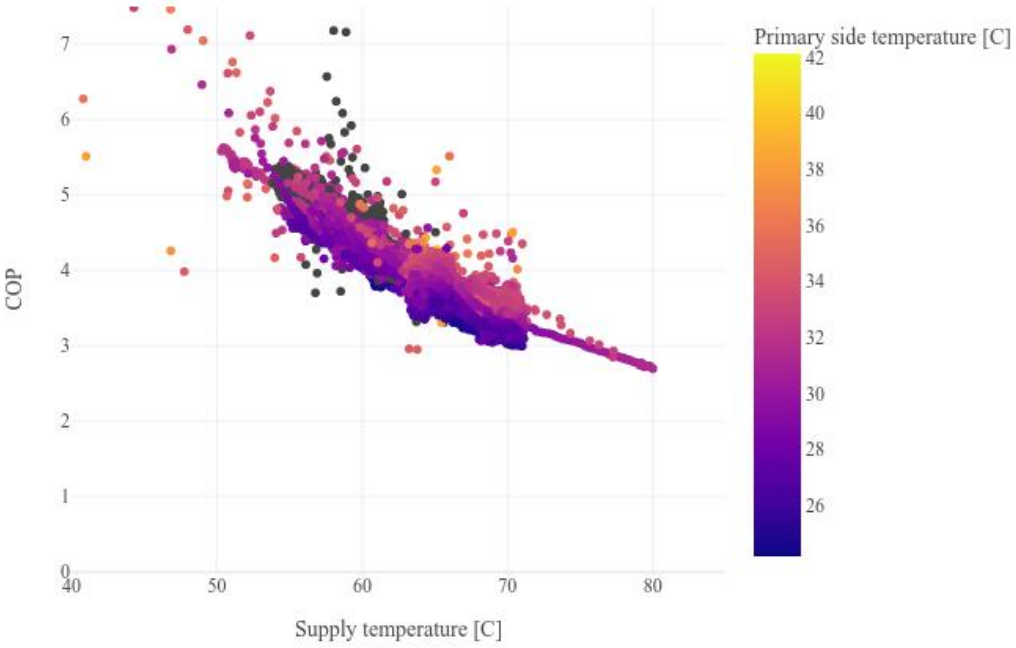

Figure 8: COP of the booster heat-pump as a function of the supply temperature delivered

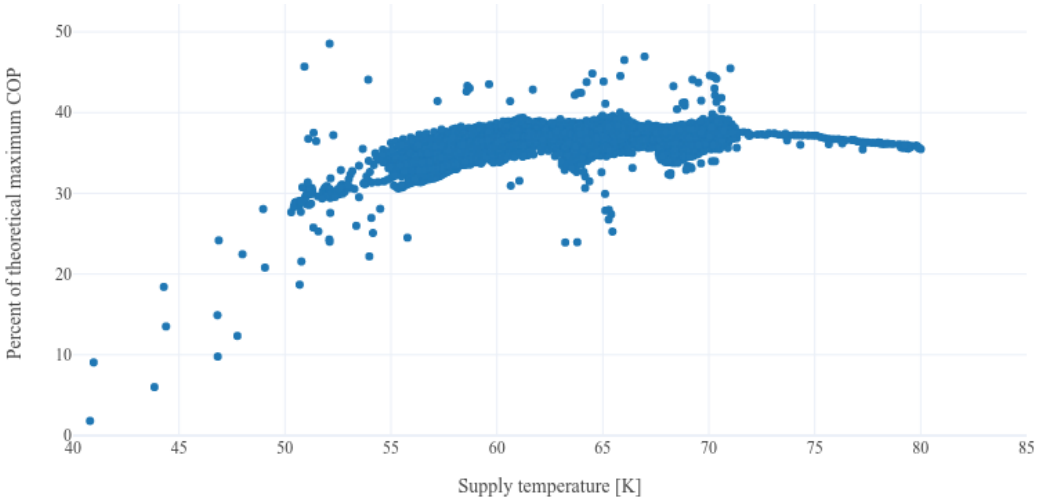

Figure 9: Percentage of Carnot COP as a function of the supply temperature

In the operating range of the booster (55 to 70°C), the COP of the heat-pump is between 30 and 40 percent of the theoretical maximum COP, which is in the low/medium-end of typical performance for vapour-compression heat-pumps (typically ranging 30-60% in experimental characterisations for such temperature spans [1]).

Then, a simple empirical model was derived from the data, to estimate the dependency of the COP to the difference between the source and the supply temperature, this dependency is shown in figure 9

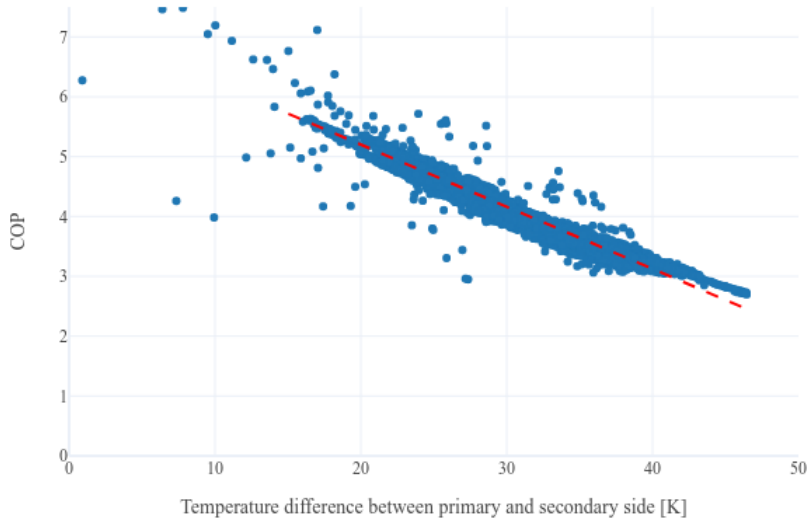

Figure 10: COP as a function of the temperature difference between the source temperature and the supply temperature (trend line: y = 7.33 + 0.1055 x)

The data trend shows that every increase of the temperature on the secondary side (at constant primary side temperature) roughly results in a decrease of the COP by 0.1. It therefore makes sense to pay careful attention to the supply temperature setpoint when optimising.

3 Control of the booster station

In this section, the control of the booster station by Neogrid and different control experiments are presented, together with learnings from the first months of operation.

3.1 Control possibilities for the heat-pump

The heat-pump was coupled to Neogrid's gateway via Modbus over a cabled RS-485 connection, which then allowed remote-control of the booster heat-pump.

To control the heat-pump, three high-level actuation options were available:

1- supply temperature setpoint control: the heat-pump regulates the supply temperature to the setpoint provided (60°C or above)
2- compressor control: either none, one or both of the compressors are activated (i.e. 0, 50 or 100% of nominal power input is used)
3- complete installation shutdown (including circulation pumps)

Where the last option was only used in the cases where the street was recoupled to the main network.

Control options for the mixer valve determining how much of the water should run through the PCM tank were also available, but have not been tested in detail, as the full flow was channelled through in our experiments so far.

This control was operated over the cloud sending schedules to the heat-pump which were regularly updated based upon the systems state. On top of this, a local rule engine running on the gateway was set up to ensure prompt fall-back in case of abnormal operation or if the supply temperature to the area fell under the required limit, also working in case the internet connection between cloud and gateway was lost.

Both supply temperature and compressor control were demonstrated in practice, with results shown in the figures of the next section.

3.2 Characterisation of the PCM tank in operation

The PCM tank is a central element for the provision of flexibility from the booster heat-pump to the electrical grid, as it decouples heat production from heat demand. A key concern of PCM-related energy accumulators is the possibility to activate them effectively and to a meaningful extend. We therefore designed experiments to assess this in our demonstrator.

Experiments were designed with a built-in safety to avoid too high drops in the supply temperature to the area (resulting in discomfort), so that the heat-pump would automatically be restarted if the supply temperature fell too low. However, we also managed to evaluate the response of the system in incident-like situations (i.e. beyond normal operation conditions), due to local loss of power in the area in a couple of occasions (snowstorms). Different scenarios are shown in figure 10 and 11.

Figure 11: Activation of the PCM tank in a period where the heat-pump was stopped 100%. In orange, the area where the phase-change in the tank dominated the response, seen by the supply temperature drop flattening out (blue curve) while the station continues delivering heat (red curve)

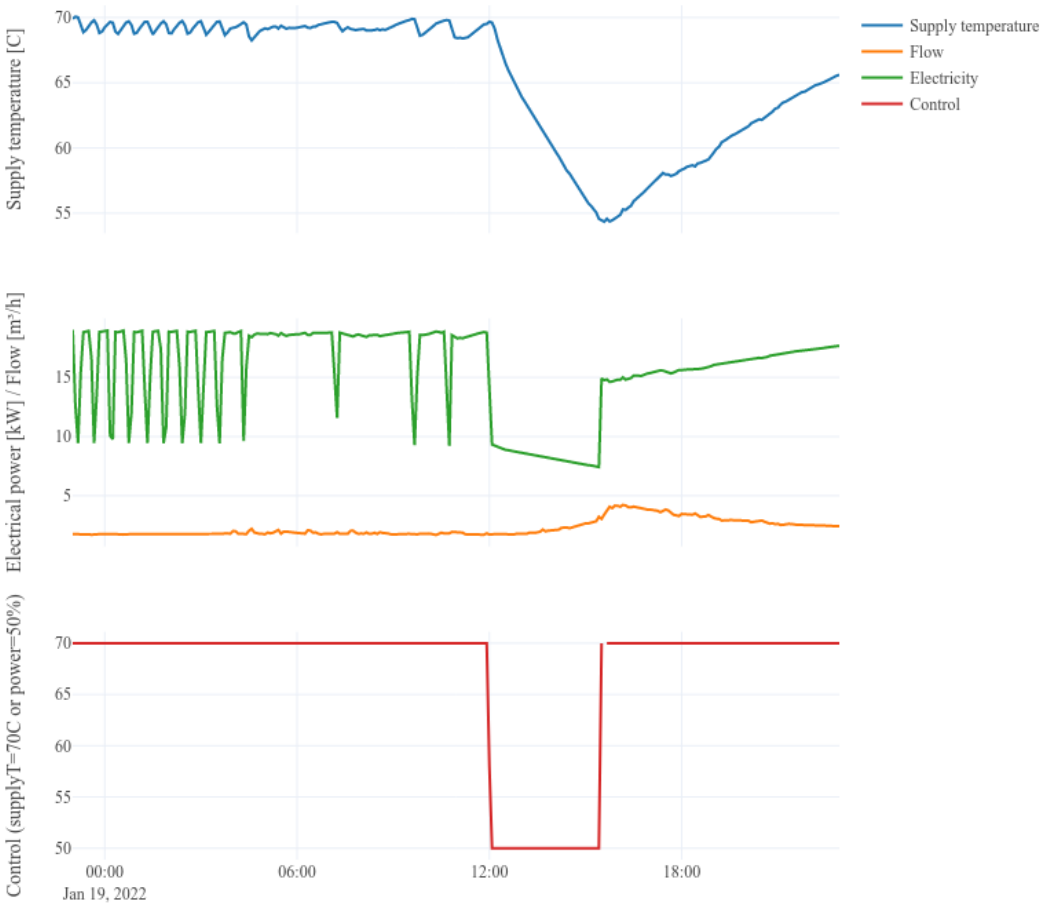

Figure 12: Reaction of the system in a period where the booster station was limited to 50% of nominal power

As highlighted by these figures, activating the PCM from the tank was not possible before reaching the limit of 55°C which should be provided to the houses in the area.

The stabilising effect on the supply temperature created by the PCM was indeed first observed when the supply temperature to the area was down to about 51.5°C (and the temperature at the output of the tank down to 53°C), as shown by the dynamic of the blue curves on Figure 11 (with a plateau during the drop around the melting point when reaching 52°C) and Figure 12 (without a plateau during the temperature drop before reaching 55°C).

This shows that there is a need for a temperature difference between melting point and water in the tank of more than 5 K for the heat transfer to take place. This temperature difference might however vary with the flow level involved, which was in the higher end (a constant 10.8 m^3/h through the tank) in this demonstration due to the requirements of the heat-exchanger towards the street. Lower flow values might require even higher temperature differences, as the heat transfer between the PCM shell and water would decrease with decreasing fluid speeds. This last aspect has however not been trialled in the demonstration.

3.3 Response of the buildings in the area to the control

Whenever the supply temperature was reduced, there was a clear trend towards an increase of flow to the street. This is an expected normal behaviour due to the regulation of the substations in the individual houses. However, this also creates challenges as the flow through the heat exchanger between the booster and the area cannot be adjusted in an equivalent manner (the pump was running constantly at nominal flow in order to reduce the temperature drop between the PCM tank and the street and thereby maximising the COP by keeping a minimal supply temperature).

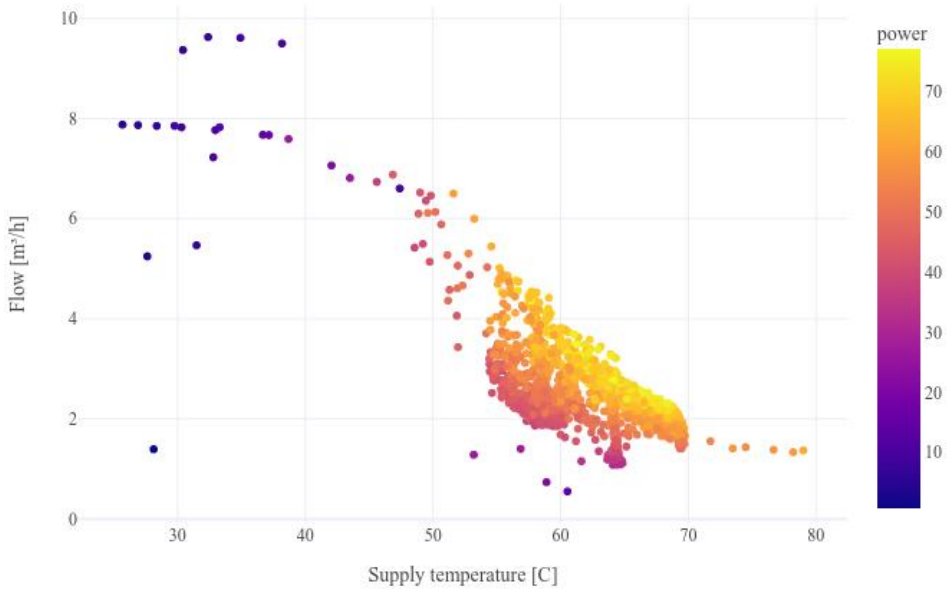

Figure 13: Flow intake of the area as a function of the supply temperature to the area, with a sharp increase below 55°C

To help with this, controllers of the individual houses will be updated to reduce their flow demand when the supply temperature is intentionally reduced (with a strategy to avoid discomfort by pre/post-charging). This has however not been implemented and evaluated at this stage.

3.4 Flexible operation of the heat-pump

The online connection to the heat-pump and connection to Neogrid's cloud allowed coupling the operation of the heat generation with electrical price conditions on the power system side. The operation of the heat-pump was therefore optimised according to the electricity price (spot prices and network tariffs), as variations in these prices were quite significant throughout the day.

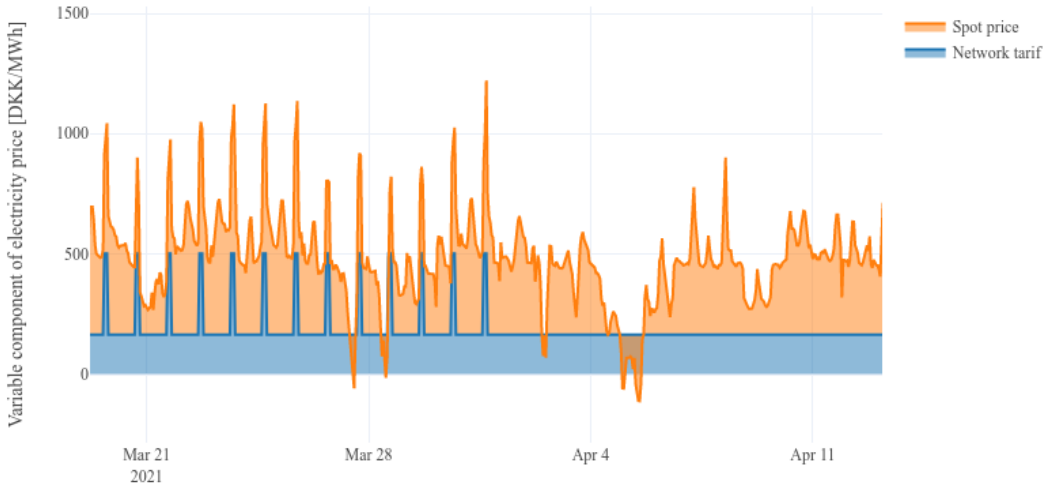

Figure 14: Typical changes in the variable part of the electricity price in 2021 (around the transition of network tariffs from winter to summer conditions, which happens on April 1st)

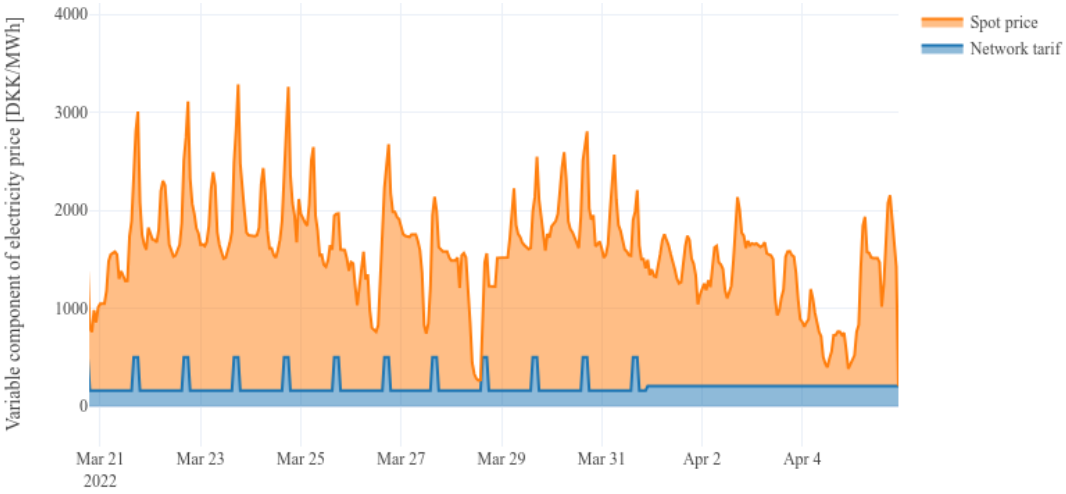

Figure 15: Typical changes in the variable part of the electricity price in 2022 (around the transition of network tariffs from winter to summer conditions on April 1st) where SPOT prices are considerably higher

A controller avoiding consumption at times where the price was high, while boosting at times where the price was lowest was implemented and demonstrated, see figure 15.

While the ambition was to converge to a detailed full-scale model predictive controller (MPC), the complexity of modelling the tank and system dynamic made it unrealistic given the measurements and resources at hand. A simplified alternative to the detailed optimisation, based upon classification of prices in 3 categories (low, normal and high price) and belonging times within a rolling window period of one day, ended up giving positive results with a much more realistic development effort.

The results of this control on the power demand of the booster station is depicted in the figure below in Figure 16 and Figure 17.

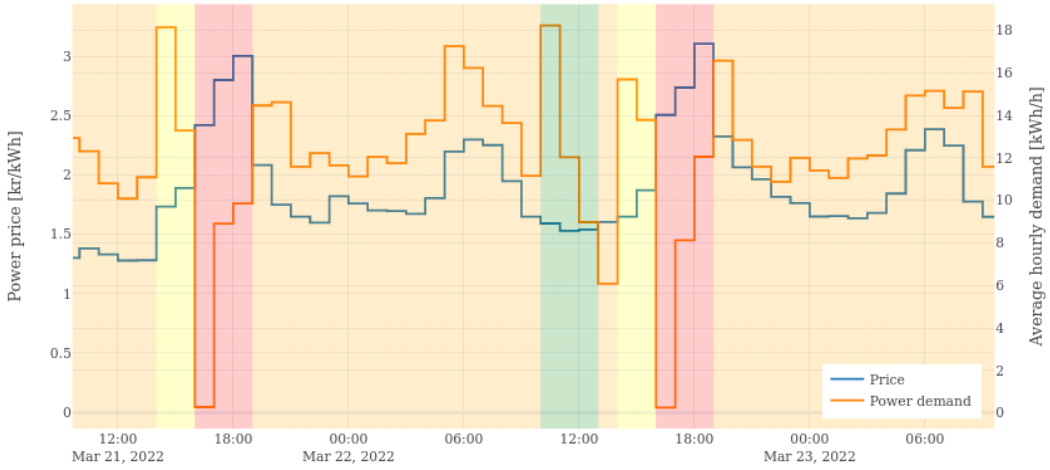

Figure 16: Example of behaviour of the optimised controller, in the context of variable electricity prices (colour code for periods: green = low price period where demand is booster, yellow = pre-high price times with preloading (also classified as low in the control), red = high price times where demand should be minimised, orange = other periods)

As seen on Figure 16, the controller reduces significantly the demand in the hours with highest price, while increasing the demand in periods with lowest price and prior to high prices. The picture also shows that even better performance could be attained by adjusting further the classification of hours, in a context where spot prices dominate the response more strongly (typically in the early morning).

This controller was compatible with the quality of supply, as it was able to maintain the supply temperature to the area above 55°C, as depicted below.

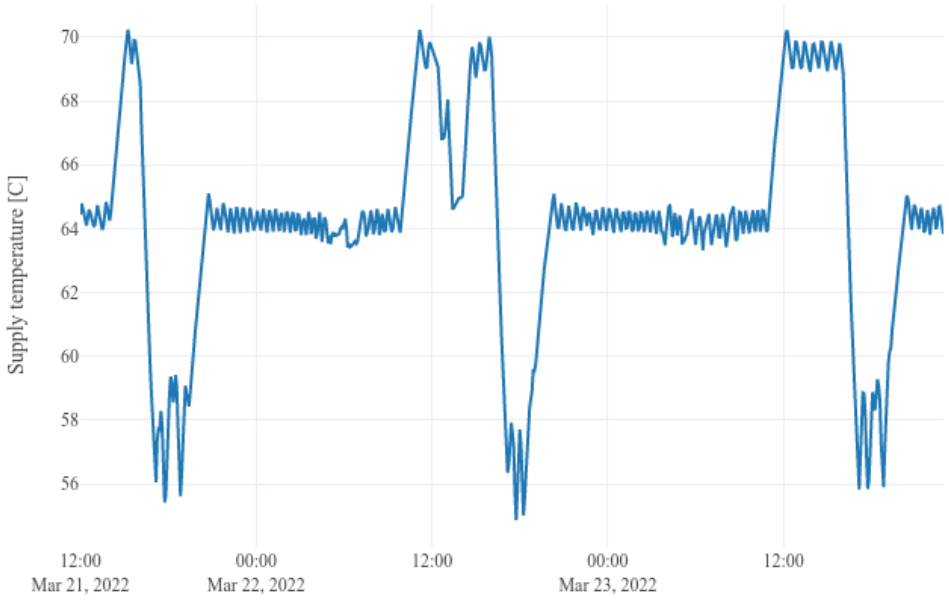

Figure 17: Supply temperature to the area during the optimised operation

3.5 Controlling the individual houses

In-house data collection was installed in 11 out of the 20 houses, out of which 6 were equipped for control via connection to the substation. For the rest of the houses, daily demand data was available from an online export from the district heating operator (Skive Fjernvarme).

Due to delays in making the booster heat-pump operational, the bankruptcy of Suntherm in early 2022 and the further challenges with the flow-relay leading to unpredictable stops of the booster after April 2022, it has not been possible to demonstrate a fully integrated operation of the booster heat-pump and the houses.

However, an optimised controller of the central supply temperature of single-family houses was developed based upon one of the houses, which had the necessary data requirements available (high resolution energy readings, as well as access to the supply temperature controller). While this controller became available too late in the heating season to be demonstrated at scale, Neogrid is confident that it will deliver value on such installations and is ready to evaluate it in its pool of houses in the coming heating season.

4 Simulation-based analyses

This section presents in-depth modelling and computer simulation analyses carried out on the setup.

4.1 digSilent simulations

This simulation illustrates the operation of booster HP with PCM based HST feeding 20 households in Citronvej. The set-up also consists of another tank that is storing return flow from DH network. The HST tank is considered to have stratification with 5 layers in the simulations, which is not a case in real system. Table II, Table III and Table IV give the parameter values towards HST and HP, which are used for simulations.

Table II: HST parameters

	Parameter
V_sto : Volume of storage tank [m3]	3.
Ra : ratio of height to diameter (H/D) of tank [pu]	2.24
U_t : Overall heat transfer coefficient of tank [W/Cm2]	0.9
Ta : Ambbient temperature in the storage room [C]	10.
Tr : Temperature of the incomming cold water [C]	35.
m_w :Total mass of hot water in the storage tank [Kg]	2055.
k_s : Thermal Conductivity - PCM - Solid State [W/m.C]	2.22
k_l : Thermal Conductivity - PCM - Liquid State [W/m.C]	0.556
m_p :Total mass of PCM in the storage tank [Kg]	1074.
Lp : Latent Heat of fusion-PCM [J/kg]	388000.
T_m : Melting temperature - PCM [C]	58.
T_f : Solidifing/Freezing temperature - PCM [C]	57.
C_pl : specific heat of PCM in liquid phase [J/Kg.K] [J/kg....	4226.
C_ps : specific heat of PCM in solid phase [J/Kg.K] [J/kg.C]	1762.
h : Convective heat transfer coeff - PCM - wall [W/m2.C]	100.

Table III: HP parameters

	Parameter
Php : Rated Power electrical of the HP [kW]	21.2
T_ope_max : Maximum operating temperature [Degree C]	70.
cos_phi_HP : Power factor of the motor driving the HP c...	0.98
C_A : Status of the heat pump [-]	0.
COP : COP of HP [-]	4.4

Table IV: HP control limits

	Parameter
T_min : Minimum Temperature allowed in the HWST [C]	45.
T_max : Maximum Temperature allowed in the HWST [C]	70.

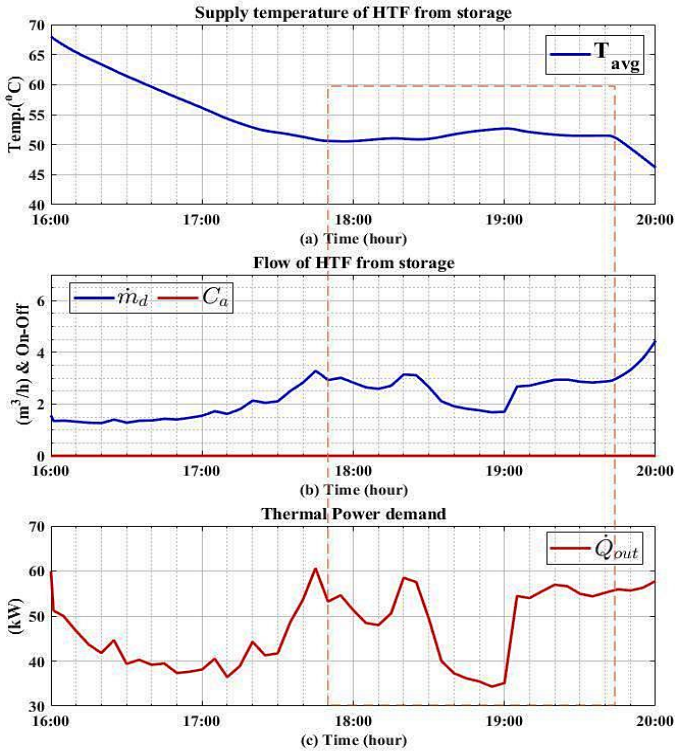

Figure 18: PCM tank characteristics from simulation results

Figure 11 and Figure 18 show the behaviour of PCM based HST observed from field and simulation results, respectively. For simulations, the temperature difference between supply and return temperatures is considered as 7°C for operation of HP. As can be seen from field result, the PCM is discharging in a period where the heat-pump is stopped 100%. In orange, the area where the phase-change in the tank dominated the response as seen the station continues delivering heat (red curve) while the supply temperature flattening out (blue curve). While the same is observed in Figure 18, where the PCM is activated when the HP is switched OFF. In Figure 18 (a) within dotted rectangular box (as compared to Figure 11), the area where the supply temperature of HTF, which is water in the present system, drops as HP is switched OFF and the phase-change in the tank dominated the response as the booster station continues delivering heat. Demand flow and

status of heat pump (ON or OFF) are illustrated in Figure 18 (b) and Figure 18 (c) shows the thermal demand supplied from the tank.

The temperature of HTF and PCM for the stratified HST are shown in Figure 19and Figure 20, respectively. The stratification defines that the PCM and HTF are not evenly warm throughout the tank but rather arranged in layers of warm/cold levels. As it can be seen, the PCM at the bottom of the tank is not able to utilize all its latent heat capacity to store energy, as this part is usually filled with cold incoming water from the return pipe. It can be a recommendation for the PCM based storage tank, to not fill it from the bottom where return pipe is connected. Figure 21 shows the flow of HTF and HP ON_OFF status. Figure 22 shows the heat pump ON/OFF status along with flow rates of heat transfer fluid from HP ($\dot{m}_s$), storge tank to fulfil demand ($\dot{m}_d$) and effective flow rate within the storage tank ($\dot{m}_e$). Figure 22 shows the state of energy (SOE) of HST. It is to be noted that when SOE is very low for the real system.

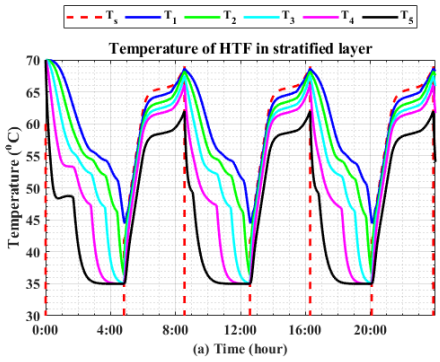

Figure 19: Temperature of HTF in the stratified HST

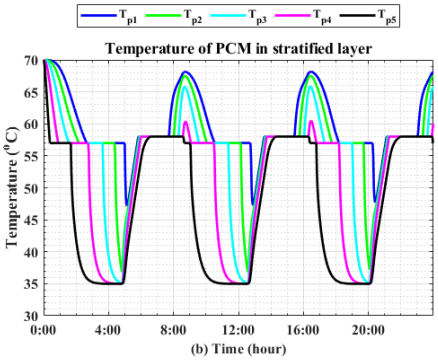

Figure 20: Temperature of PCM in the stratified HST

The supply from storage tank and demand is directly supplied to the consumer through heat pump. So, depending upon the size of HP, storage and demand, the optimal SOE can be determined. If HP alone can handle the demand, then the SOE can go up to 0% in the tank. The energy stored in the tank is not reaching its 100% due to the mandatory temperature difference (ΔT) between supply and return temperatures. Figure 23 shows the thermal input/output of the HST.

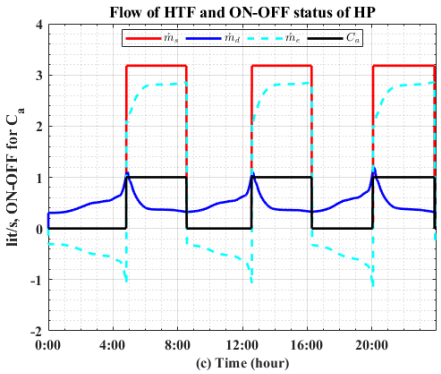

Figure 21: Flow rate of HTF and HP status

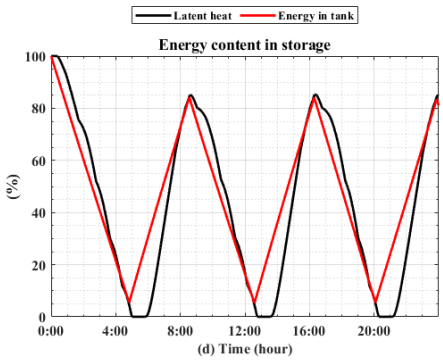

Figure 22: SOE of HST

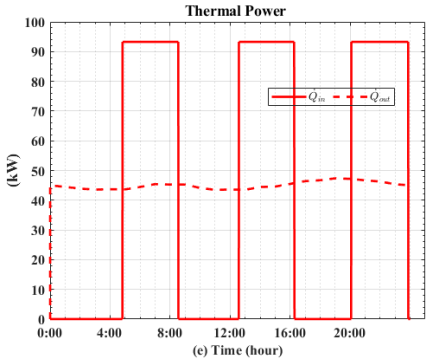

Figure 23: Thermal power IN/OUT of HST

4.2 Modelling of PCM Storage and simulation results

The average model of PCM storage tank is modelled based on eq.(1), where the temperature of heat transfer fluid (HTF) inside the storage tank is uniform.

$$\frac{C_f dT_{avg}}{dt} = C_w \dot{m}_s (T_s - T_{avg}) - C_w \dot{m}_d (T_{avg} - T_r) - \dot{Q}_{PCM} - \dot{Q}_{loss} \quad \text{eq.(1)}$$

$C_f = m_w C_w$ = Thermal capacitance of HTF [J/K]
C_w = specific heat capacity of HTF (water) [J/kg.K]
$C_w \dot{m}_s (T_s - T_{avg})$= Net rate of energy transport for charging storage tank
$C_w \dot{m}_d (T_{avg} - T_r)$ = Net rage of energy flow during discharging of tank
$\dot{m}_d$ = flow rate of heat transfer fluid for discharging storage tank [kg/s]
$\dot{m}_s$ = flow rate of heat transfer fluid from source for charging tank [kg/s]
m_w = mass of water in the tank (kg)
$\dot{Q}_{PCM}$= net rate of energy transport for charging/discharging PCM storage
T_{avg} = average temperature of HTF in storage tank [K]
T_r = Temperature of return HTF from heat sink [K]
$\dot{Q}_{loss}$ = Net rate of heat loss from the storage tank.

The discretised model of thermal storage tank, with n number of horizontal layers with the equal mass of HTF and PCM material in it, Is represented in Figure 24 (a,b). The energy balance within each discrete layer is well presented in Figure 24 (b)The exchange of thermal energy from PCM is only with the HTF in each discrete layer. The modelling of discretized layers for the HTF is based on

$$\begin{aligned} m_i C_w \frac{dT_i}{dt} = {} & \dot{m}_{in} C_w (T_{i+1} - T_i)\delta_{(i \neq n)} + \dot{m}_{in} C_w (T_{in} - T_i)\delta_{(i=n)} \\ & - U_t A_{st} (T_i - T_a) \\ & + \frac{A_q \lambda_w}{z} \left[(T_{i-1} - T_i)\delta_{(i \neq 1)} - (T_i - T_{i+1})\delta_{(i \neq n)} \right] \\ & - U_{pcm,i} A_{pcm,i} (T_i - T_{pcm,i}) \end{aligned} \quad \text{eq.(2)}$$

$A_{pcm,i}$= effective heat transfer area of PCM[m^2]
A_{st}= surface area of the side wall of each discrete layer [m^2]
A_q= Horizontal surface area of the storage tank [m^2]
$\dot{m}_e = (\dot{m}_s - \dot{m}_d)$: effective flow rate of HTF inside the tank [kg/s]
m_i= mass of HTF in each discrete layer [kg]
T_i= Temperature of HTF in each discrete layer [K]
$T_{pcm,i}$= Temperature of PCM in i^{th} layer [K]
$U_{pcm,i}$= overall heat transfer coefficient of PCM in i^{th} layer[$W/m^2.K$]
z= Thickness of each discrete layer [m]
$\delta_{(X)} = 1$ for all the conditions defined by term X is true, else 0.
λ_w= effective vertical heat conductivity of water (W/mK)

Available data on PCM and Storage:

- Storage Volume: 3000 L
- Number of elements (HeatSel): 110 per 100 L
- Water content in tank: 2055 L
- PCM type: ATS 58
- 1 heat seal with plastic cover = 382 ml
- 1 heat seal without plastic cover = 334 mL
- Density of pcm = 1.3 kg/L
- Storage capacity PCM (50 – 65°C): 240 kJ/kg

Note: As per the data sheet, latent heat capacity for the temperature range (50-65 oC) is 240kJ/kg, whereas, in simulation, the phase change is considered at a constant temperature. Thus, there is extra heat as sensible for a 15-degree temperature difference of PCM at the temperature range of 50-65 °C. Thus, Sensible heat stored in PCM for delta T (65-50=15) is 1x3000x15=45000 J/kg.K

- latent heat for simulation = 240000-45000=195000 kJ/kg
- Calculated value
- Heat seal in tank = 3000-2055=945 L
- No. of heat seal = 945/0.328 = 2474
- Volume of PCM only = 2474/0.334 = 826 L
- Mass of PCM in the tank = 826x1.3 = 1074 kg

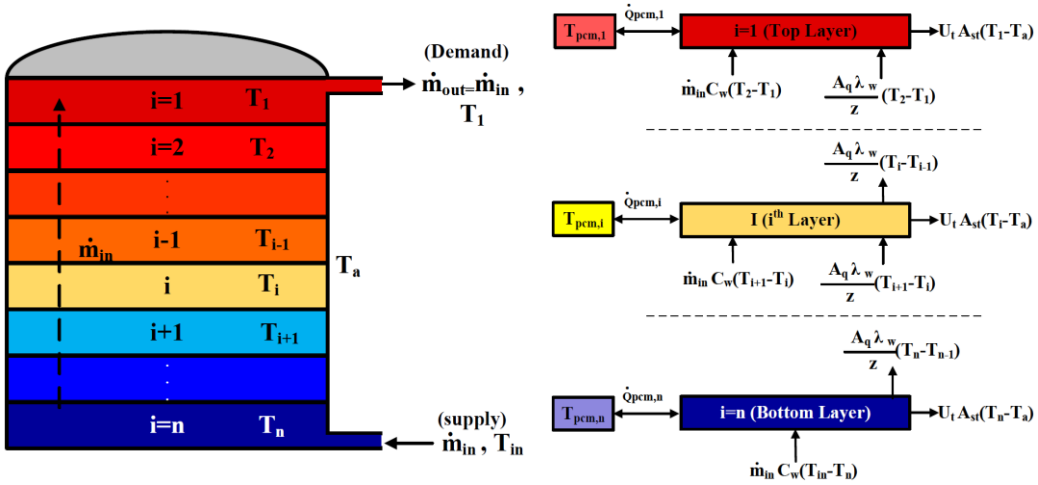

(a) (b)

Figure 24: (a)Stratified PCM based thermal storage tank; (b) Stratified PCM based thermal storage tank with n layers and flow variables

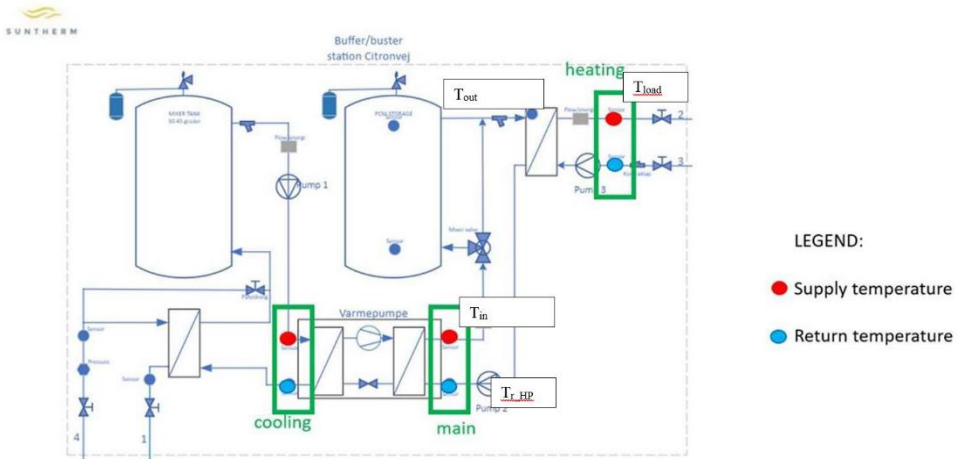

Figure 25: Booster HP setup with thermal storage and temperature legend

Figure 25 illustrates the booster HP setup with thermal storage. The block frame of the complete thermal system developed in DSL-PowerFactroy is shown in Figure 26. The thermal system consists of a measurement unit (supply voltage), schedule unit, thermal demand profile (thermal demand), PCM-based storage system, heat pump unit, the control unit for HP activation, feedback unit to maintain the temperature of HTF flow from HP, and finally the electrical load to the power system.

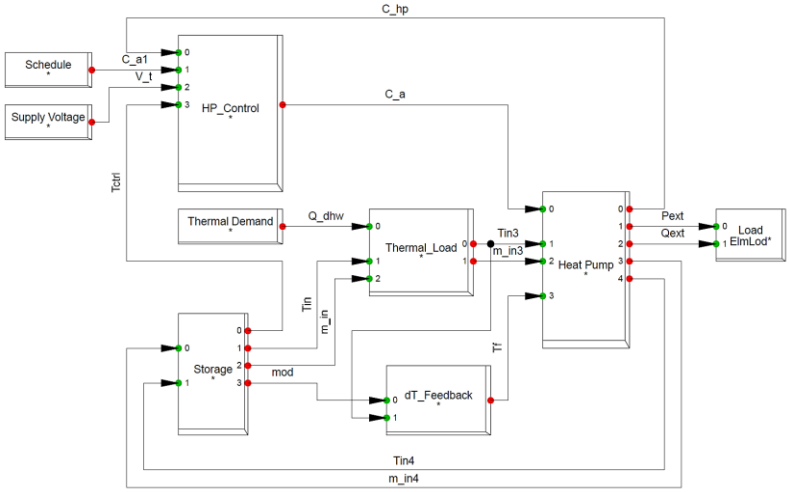

Figure 26: System architecture modelled on DIgSILENT Powerfactory

Measurement unit: supply voltage block measures the voltage of the power system at the point of common coupling of HP (V_t). This measurement is used by 'HP control' unit as a part of demand response to regulate the distribution system voltage by varying the operating power of HP.

Thermal demand profile: thermal demand block provides the characteristic profile of thermal energy supplied to the consumer (Q_{DHW}).

Schedule unit: this unit provides the operating schedule of HP (C_{a1}). The operating signal can be based on individual preference or optimized solution based on estimated demand and electricity price. The signal (C_{a1}) can be either discretized value (0-1 for ON-OFF) or per unit value based on the operating power level of HP.

Control unit: the control unit block (HP Control) is setup to performs the logical evaluation of various parameters to determine the operational status of HP as an output (C_a) block. The control scheme of the heat pump is based on two levels. The first level of control comes from the scheduled unit (C_{a1}). The second level of control will manage the operation of HP concerning the state of energy of storage, HP dynamics, supply voltage and users' priority. This two-level control ensures the reduction of forecasting errors through feedback to the first level from the second level control and supports local node voltage regulation. This part of control unit is not yet applied in the simulation yet, and is considered for further evaluation in future.

Operating temperature of HP: The output temperature of HP is maintained by the block 'dT Feedback' unit. This is an inbuilt function of HP which maintains the temperature difference between the incoming and outgoing temperature of HTF. This unit continuously monitors the temperature of HTF from the bottom of the storage tank to the HP and sends the feedback (T_f) to determine the output temperature of HTF to the storage. This temperature difference helps to maintain the constant flow rate of HTF from the HP.

Heat pump: This unit represents the HP dynamics based on [4]. The thermal power produced by HP is calculated using .eq.(3) and the reactive power consumed is based on eq.(4) where COP is the coefficient of performance, P_{HP} is the electrical power rating of HP and θ is the load angle. Pext and Qext are the active and reactive power consumed by

HP. The flow rate of HTF from the HP (m_s) (which is constant) and the temperature of HTF (T_s) are sent to storage.

$$\dot{Q}_{heat} = COP.P_{HP} = m_s C_p(T_f - T_{in}) \quad [W] \quad \text{eq.(3)}$$

$$Q_{HP} = P_{HP} \tan\theta \quad [VAR] \quad \text{eq.(4)}$$

Load: this unit represents the electrical load of HP as active and reactive power to the power system.

Storage: this unit represents the PCM-based thermal storage system. Two different models of storage can be selected based on the requirement. One is an average model where temperatures of HTF and PCM are uniform through the storage. The second is a discrete model of storage where temperatures of HTF and PCM are determined for each discrete layer of the storage. The output signals from the storage are: Tctrl- feedback of temperature for control, mod: working mode of storage (average or stratified), and Trhp-return temperature of HTF from the bottom of the storage to HP.

Table II, Table III and Table IV give the parameter values towards HST and HP, which are used for simulations. The flow of HTF is maintained at 10.8 m^3/h. The analysis is made only for discharging the thermal storage tank. A comparison between the discrete and average model of the PCM-based thermal storage system is presented in Figure 27. The result is further aided with the real measurement from the field. It is worth noting that the field measurement is performed at the heating unit T_{load} and compared with measurements from point T_{out} for simulation models as shown in Figure 25

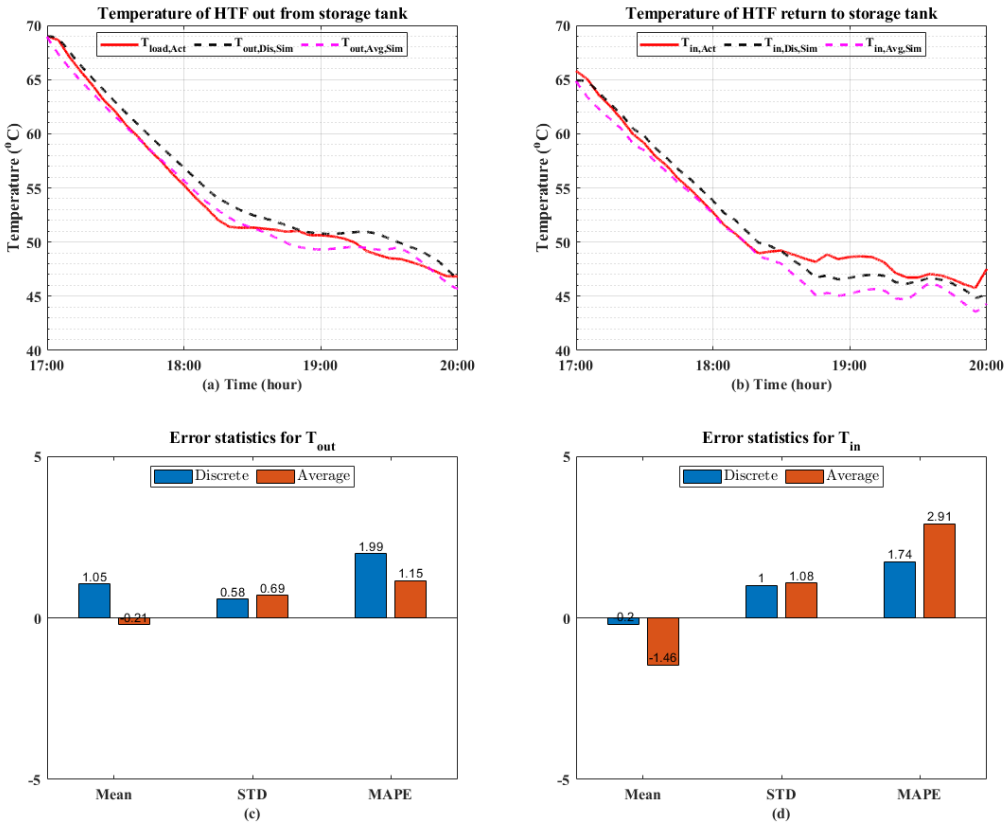

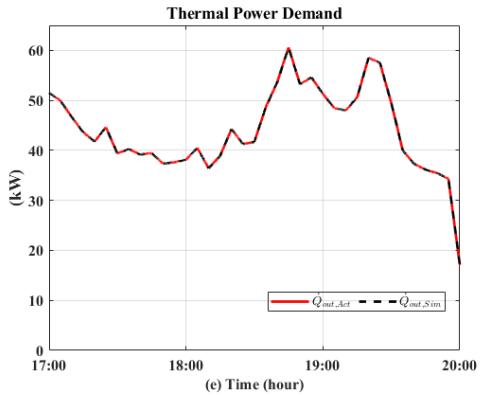

Figure 27: Comparison of results between actual measure data (Act), and simulated data results (Sim): Dis:- for discrete model and Avg:-for average model of the thermal storage tank. (a)-(b): Temperature of HTF out from storage tank T_{load}/T_{out} and return temperature T_{in} respectively; (c)-(d): errors in simulated value of T_{load}/T_{out} and Tin respectively; (e):Thermal Power Demand-actual and simulated

Figure 27a illustrates the temperature of HTF out from the storage tank for real system ($T_{load,Act}$) and simulated models which includes discrete ($T_{out,Dis,Sim}$) and average model ($T_{out,Avg,Sim}$). Similarly, Figure 27b illustrates the temperature of HTF return to the storage tank (T_{in}). Figure 27c and Figure 27d represents the statistical data on the error such as mean, STD and MAPE of T_{out} and T_{in} respectively for both the models. Figure 27e shows the thermal power demand.

Since the flow of HTF is high (around 10.8 m^3/h) and also from the bottom of the storage tank, average model of the storage tank shows smaller error compare to discrete model (Figure 27c) for T_{out}. However, the temperature gradient of T_{out} (Figure 27 a,b) at the beginning of discharge (17:00) and towards the ending of discharge is well aligned with the discrete model, which is an import parameter for On/Off operation of HP based on temperature measurement.

4.3 Python package for PCM simulation

The following describes the OpenTerrace framework developed by Aalborg University in synergy with the Serene H2020 project[1]. The official website containing all package details is available at https://openterrace.github.io/openterrace-python/. While OpenTerrace is a flexible framework that allows users to modify and extend it capabilities, the following will focus on a cylindrical 1D storage tank with 1D PCM capsules (approximates as hollow spheres) as bed material. The storage tank filled with PCM modules is shown in Figure 28.

[1] https://h2020serene.eu/

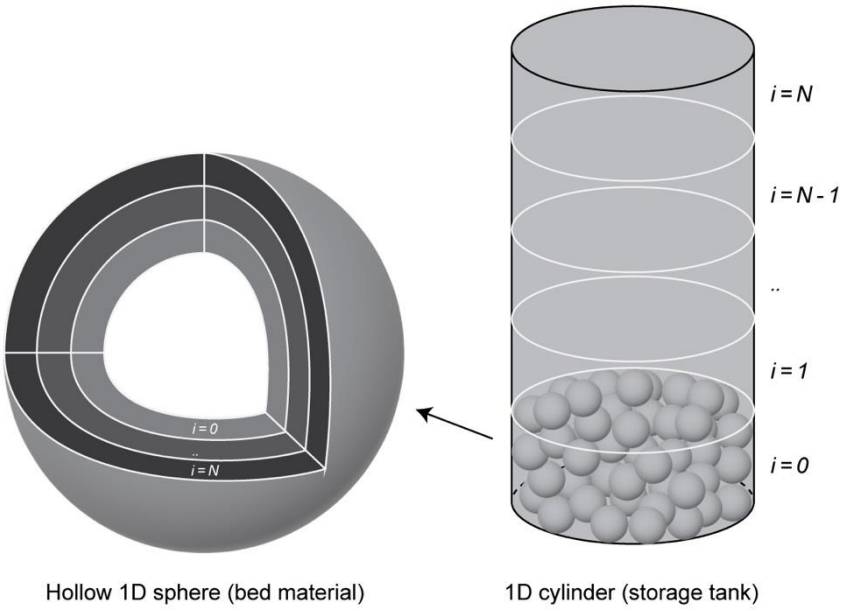

Figure 28: Schematic of a PCM capsule represented by a discretised 1D hollow sphere and the 1D cylindrical storage tank.

The storage tank

The storage tank (cylindrically shaped) is discretised in one dimension with *N* cells from the bottom ($x = 0$) to the top ($x = h$). Each cell has a user-specified volume fraction of bed material (PCM capsules), which may vary spatially throughout the storage tank. This functionality can be used to emulate a storage tank partially with PCM capsules. Within each cell in the storage tank the PCM capsules are assumed to have the same spatially varying temperature distribution.

The PCM capsules

Each PCM capsule is discretised with cells from the centre ($r = r_{\mathrm{inner}}$) to the outer surface ($r = R$). The actual PCM capsules are of a complex irregular shape, which is three-dimensional. In the OpenTerrace framework the idea suggested by Grabo et al [2] is used to map the actual geometry into a hollow sphere while ensuring both equal volume and outer surface area.

Figure 29: A PCM capsule consisting of outer plastic shell and PCM material inside.

Model limits

a) Storage tank is modelled as a 1D cylinder. In reality flow develops are creates a non-uniform flow profile due to the non-slip condition at the wall. In reality the lower fluid velocity close to the walls of the cylinder results in lower heat transfer rate as a result of the lower heat transfer coefficient.
b) PCM capsule approximated as a hollow 1D sphere. Even though the volume and outer surface area are the kept constant in the transformation, the area function differs between the two. A fully 3D model of the PCM capsule would be required but takes significantly more time to solve.
c) Flow is assumed to enter the storage tank uniformly. In reality a jet might be present that would effectively cause enhanced mixing in the inlet region.

Code verification

To ensure correct code implementation and sufficiently small spatial and temporal discretisation steps, various benchmark cases are run. These can be found here: https://github.com/OpenTerrace/openterrace-python/blob/main/openterrace/tests/

These cases represent extremas where analytical solutions exist and used to simply verify the code implementation. They include pure diffusion in a solid sphere and pure advection of a temperature field in an empty storage tank. As the figure below shows, the OpenTerrace modelling framework accurately predicts transient heat transfer in a sphere down to within 1% with 50 discretisation points.

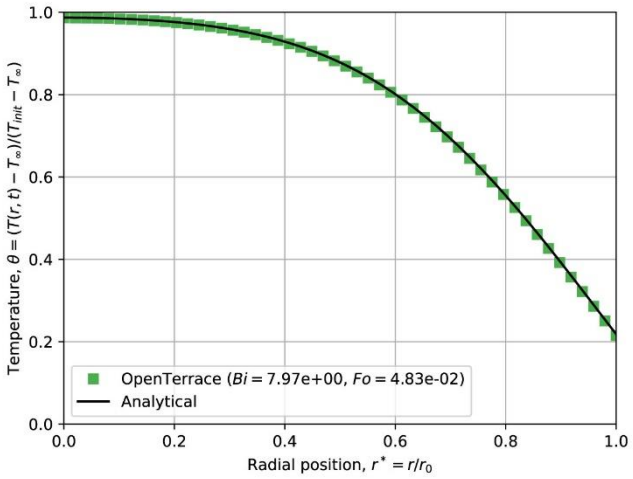

Figure 30: Code verification for heat diffusion in a sphere.
Both the Biot (Bi) and Fourier (Fo) are non-dimensional numbers.

More information about how to get started with OpenTerrace is given at https://openterrace.github.io/openterrace-python/user-guide/get-started/

while various tutorials can be found at https://openterrace.github.io/openterrace-python/tutorials/ .

5 Learnings and challenges of real-world implementation and operation

When implementing and operating the system in practice, a number of challenges were encountered, which are presented in this section.

5.1 The heat demand of the area had been underestimated

Once the station was operating and demand data from the houses was imported on a regular basis, an estimation of the distribution heat losses on the street became possible. The sum of household demands was estimated from the sum of the households for which the data is available, and an estimation of the ones for which it was not (based upon the median of the other houses).

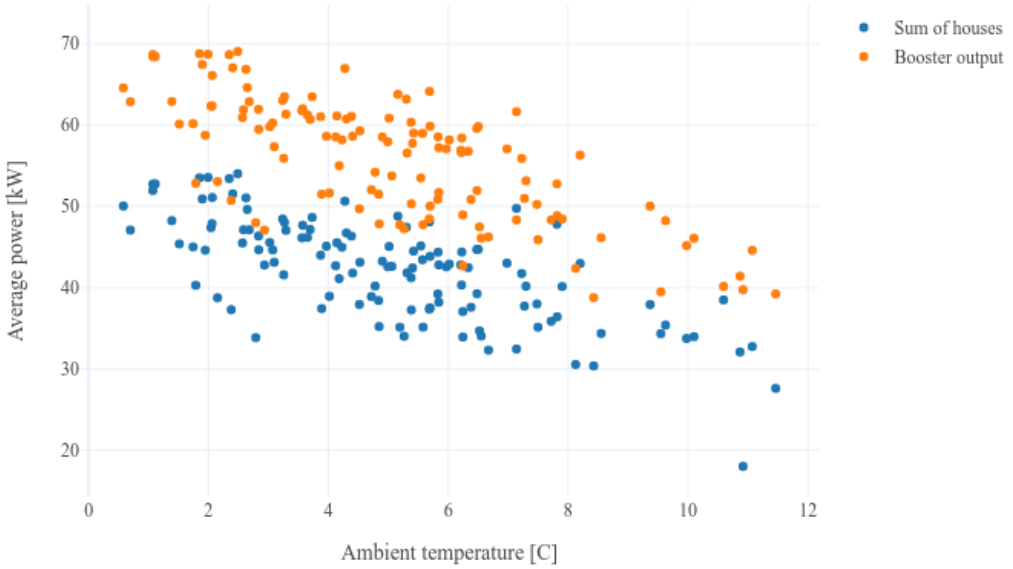

Figure 31: Actual heat demand profile of the area (winter 2021-2022) based upon daily values, with sum of demands of houses and heat delivered by the booster

When comparing expectations of the power demand of the area (Figure 2, based upon the sum of household demands) and the actual one (Figure 31), it turns out that the average demand in the area is considerably higher (by around 25%) than expected.

Distribution heat losses were then estimated by looking at the difference between the energy delivered by the booster station and the estimated sum of the demands of the houses. Resulting timeseries of these losses are given in Figure 32 and Figure 33 below.

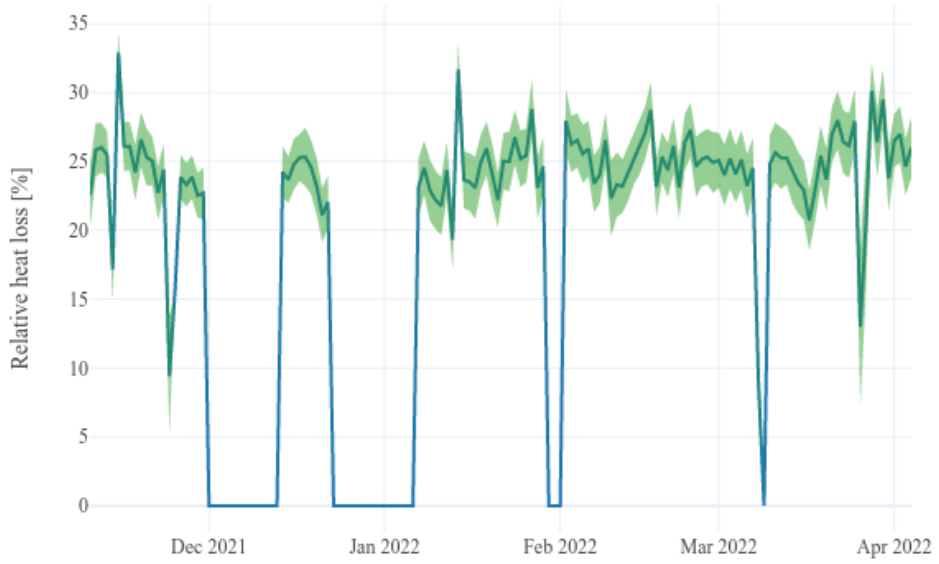

Figure 32: Estimation of relative heat loss in a winter period (0 indicates no operation of the booster)

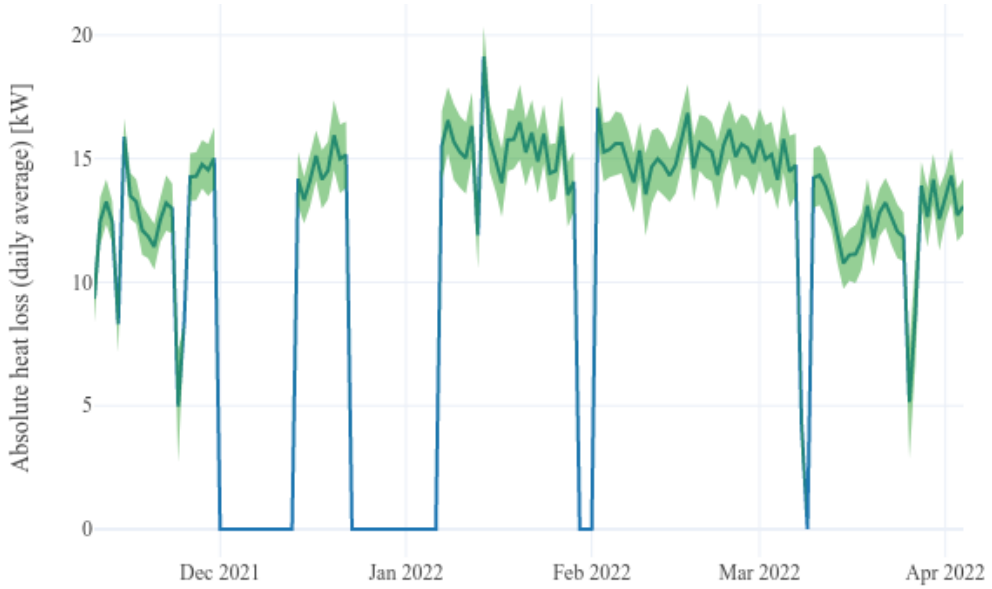

Figure 33: Estimated (absolute) heat loss in the area in a winter period (0 indicates a period where the booster is decoupled)

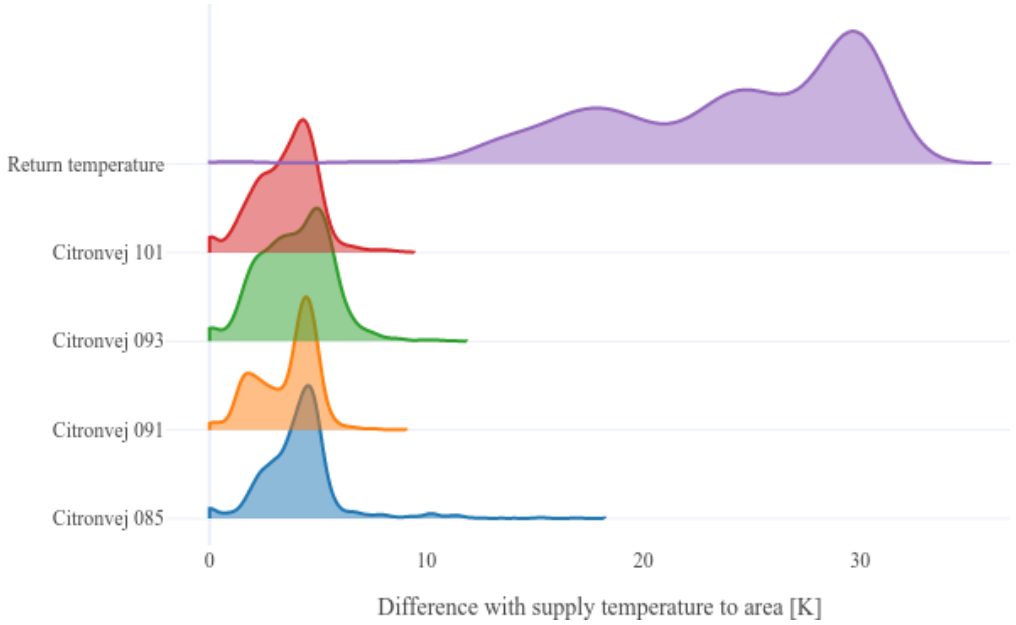

Figure 34: Distributions of the difference between the supply temperature from the booster station and the supply temperature received at household level (the difference with the return to the booster is also provided for context on the first purple ridge line). This quantifies the magnitude of the heat loss in the street, as well as the variations from house to house due to their different distance and pipe connection to the booster station.

These three figures show that in winter conditions, the temperature drop between the station and the houses down the street is in the range of 5 K, with an absolute heat loss of 10-15 kW and a relative heat loss of 20-30 %. When it comes to the heat-loss, it is however worth mentioning that these estimations have some uncertainty, as data was missing for 4 of the houses (out of 20). The gap was filled using an average of the other 16, which can bring significant error in such a small sample.

It had however not been possible to get a more precise estimate, as a local measurement of flow and supply/return temperatures was not available prior to the deployment.

This discrepancy can be explained by the losses in the street pipes, as well as additional losses introduced by the new system. While this part is no surprise, the magnitude of these losses is nevertheless in the higher end. A learning here is therefore to include higher local losses (with at least a 25% margin) on top of the sum of demand in the design phase of future installations.

5.2 Measuring the heat output of the heat-pump is challenging in high flow conditions

A specific challenge encountered with the energy meters (SHARKY 775 from Diehl, a classic heat-meter in Denmark) was that the temperature difference across the meter on the secondary side of the heat-pump was often too close to the meter's limit (3 K) given the high flow in the loop (in the range of 10 m^3/h).

As a consequence, we have not been able to evaluate the heat losses of the tank and equipment, since the energy output of the heat-pump was typically measured to be lower than the energy delivered to the street (which was a more reliable measurement within the operating range of the meter).

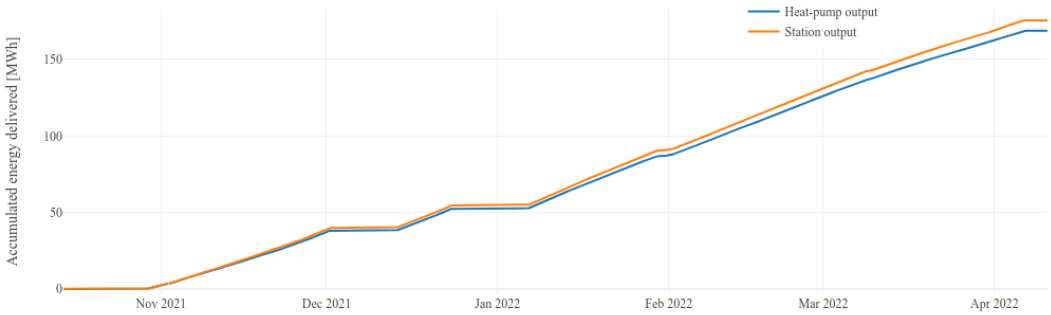

Figure 35: Comparison between measured energy delivered by the heat-pump (blue) and by the booster station as a whole (orange). If these measurements were accurate, the tank would have negative losses (of about 4%), which does not correspond to a physical reality.

Similarly, we have not been able to use these measurements to accurately evaluate the state of charge of the tank, which would have been very valuable for advanced model-predictive control development.

5.3 The estimation of the PCM tank's state of charge is a major challenge

When it comes to estimating the state of charge of the tank, this was particularly difficult to do due to a significant hysteresis from the PCM around the PCM melting point (i.e. no one-to-one equivalent between tank temperature and state of charge) and the operating limits of the energy meters before and after the tank and exchanger (where the difference accumulates over time, as discussed above in 5.2).

An alternative strategy for evaluating the state of charge of the tank then consisted in adding a temperature sensor before and after the tank, so that we could estimate the power intake/output from this difference and the flow rate.

Given that the PCM state change implied a volume change for the PCM material, we considered whether using a pressure measurement in the tank could help estimating this state of charge when the temperature is close to the melting point. We however did not get a chance to evaluate this point.

5.4 Limited flow in the line used as primary supply to the heat-pump

The heat-pump was coupled to a buffer tank on its primary side, to allow for fluctuations of the flow in the line connected to the primary side. However, we observed that the flow in the local return line (supplying the primary side) was much lower than expected, which has brought a number of challenges, including a reduced COP for the heat-pump

and maximum heat-output delivered which was lower than expected. This implied that in the coldest days, the heat-pump needed to run at full power nearly all day.

However, this challenge is specific to our demonstrator, which was installed on a return line of a rather small area. In practice, this challenge would not be met in a situation where the booster is actually installed on a well-dimensioned dedicated low temperature supply line.

5.5 Insufficient margin between the PCM's melting point and supply temperature requirement

The usage of a heat-exchanger between the PCM tank introduced a temperature drop between the heat-pump and the street, which was minimised by operating at constant maximum flow within the booster loop. In winter conditions, this temperature drop is around 0.5 K with peaks over 1 K in periods with higher flow. This is a rather small figure, which however has a small impact on both the COP and a stronger one on the possibility to exploit the PCM due to the need to keep the supply temperature to the area well above 50°C and have enough temperature difference with the PCM's melting point to ensure adequate heat transfer.

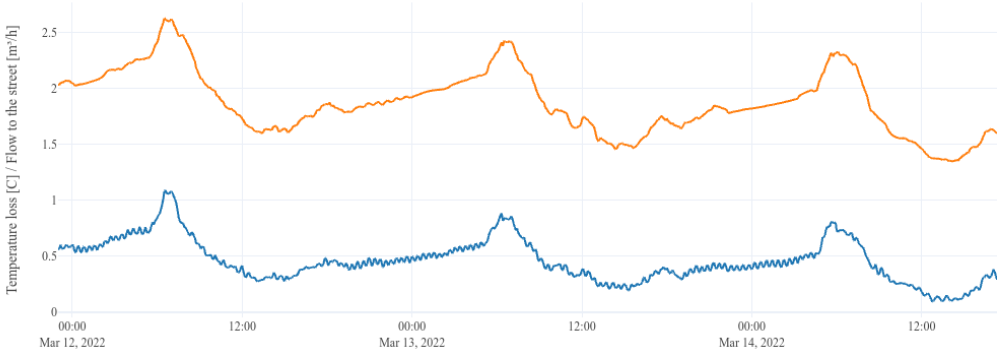

Figure 36: temperature loss (blue) through the exchanger and flow (orange) on its secondary side (with hourly averaging)

5.6 Erratic safety triggers are a major challenge in a distributed setup

Another challenge encountered was the safety check of the heat-pump, which gets triggered if the flow on the primary side stops in order to protect the installation. Whenever this safety is activated, the heat-pump stops and blocks until a manual reset is triggered on site. While this is an appropriate requirement in a building where operators are constantly present (e.g. industrial production installations), this is a significant drawback in a decentralised system with units scattered around a municipality where technicians need to be dispatched. This is especially critical in case of a blackout in the system, as all installations in an area would get triggered in a short period of time and result in a correlated surge of action for the operation team, which is also likely to otherwise be loaded with other equipment that needs to be restarted. Alternative ways of safely reinitialising

a fleet of booster heat-pumps should therefore be evaluated, which is likely to involve hardware design updates.

5.7 Limitations in setpoint ranges introduce operational challenges with PCM

The chosen heat-pump can only operate in two modes: either according to a temperature setpoint, or with 0, 1 or 2 active compressors. An operation based purely on temperatures might have been advantageous from a control stability and robustness perspective. However, this was not compatible with the PCM's characteristics, as the heat-pump's software would not allow a setpoint below 60°C, which was above the PCM's melting point. With our choice of material, being able to have an acceptable setpoint range starting from 50°C would have been more adequate.

5.8 A hierarchy of controllers with low-level bypass was required in such a multi-stakeholder setup

In this setup, a variety of stakeholders were involved, with different responsibilities. In particular, Suntherm was responsible for the safe operation of the booster station as well as the security of supply[2], while Neogrid was responsible for the online data collection and optimisation of the control.

Given that the heat-pump required a complex switching between modes (i.e. several signals had to be switched at the same time to achieve the desired behaviour), a hierarchical solution was required, where possibilities and responsibilities at each level were transparent and well-defined. As part of this hierarchical design, each level should have the possibility to disable influence of upper levels (without them disturbing operation in that case) and these levels should be divided according to responsibilities (upper levels for optimisation, lower levels for safety and security of supply).

In our case, the stack ended up looking like:

[2] The project partners were only responsible for the security of supply at times when the area was coupled to the booster station. When the street was coupled back to the main district heating network, this responsibility went back to the district heating operator. In this setup, the district heating operator was also given access to the well and its valves, so that it also could enforce a bypass of the booster station.

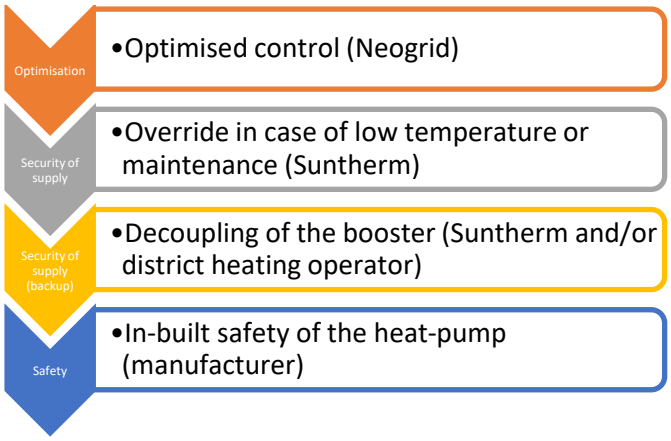

Figure 37: Hierarchical controller structure for the booster station in the demonstrator

This hierarchical control was implemented using Neogrid's rule-engine (on the local gateway) for the upper 2 levels, while the 3rd level was a manual process and the 4th operated on the heat-pump itself (as a part of its original firmware).

This division in such 4 levels can typically be realised for any installation in the future, except for the fact that the decoupling of the booster should be replaced by activation of some sort of backup capacity (as the temperature on its primary side would be too low to supply the area). In such a case, it would be important to allow for automatic (or at least remote) decoupling of the booster and activation of backup when needed, in order to avoid having to send a technician on site when a failure happens and react fast before comfort is degraded for the end-users.

5.9 Flow requirements for the primary side of the booster must be co-ordinated with district heating operation and dimensioning

In the second half of 2022, the demonstration was started again after the flow-switch issue was corrected. However, the heat-pump was not able to operate for long, as the flow in the return line used as a heat source had significantly decreased and the temperatures on the primary side in boosting conditions dropped by about 20 C in boosting conditions. This meant that the booster was reducing the temperature of this water too much (below 10 C), compared to what it was designed to operate with, which implied by inefficiencies but also security risks (due to the risk of freezing as water approached 0 C) which its local control was designed to prevent.

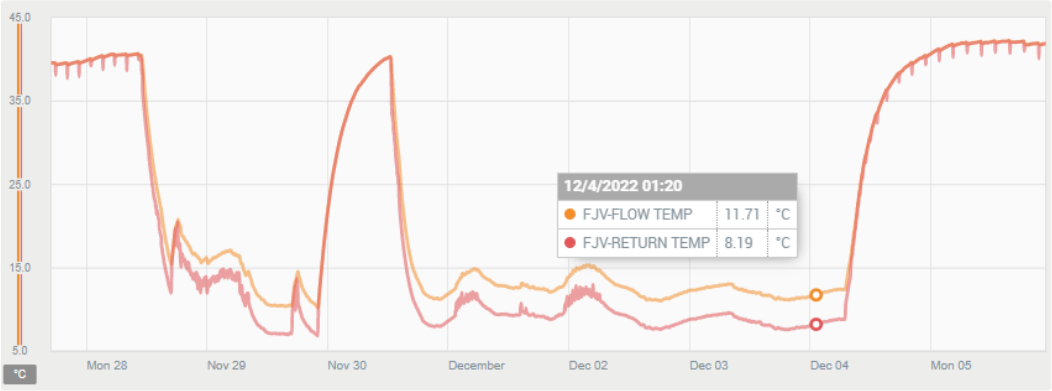

Figure 38: Example of the temperatures reached on the primary side of the heat-pump after the flow of the return line dropped (increases correspond to periods where the booster was switched off and the water in the primary tank got heated up again by the return line)

Unfortunately, this irreversible flow reduction in the return line was beyond the control of the project partners and due to the operation of the buildings on the line[3] and control of the district heating. Therefore, the demonstration of the booster had to come to an end, without gathering results of a second winter.

This point is of course more specific to the usage of a local return line, rather than a dedicated low—temperature supply line. It however illustrates the importance of providing sufficient flow in order to ensure the feasibility of boosting at adequate temperature levels for the heat-pump design.

[3] A potential explanation could be the implementation of strong energy conservation measures in response to energy price increases due to the geopolitical situation, but we were not able to confirm this.

6 Conclusion

The project was able to successfully implement and operate a booster heat-pump supplying a residential street in Denmark as highlighted in this report summarising the findings, achievements and learnings of the demonstration.

When it comes to hardware, the partners managed to design, build and operate a

booster station with a PCM storage tank providing heat to a group 20 houses from a cold temperature primary source. The station was operated during the winter of 2021-2022, where it provided the houses with heat over longer periods.

Performance of the PCM was characterised in-situ, where energy was loaded in and out of the material in the tank, while also highlighting the need for a higher melting point in similar future applications. Based upon these results and given the modelling complexity and cost of the solution with PCM, it does therefore not seem to have a strong operational advantage over a larger water tank with same heat-capacity for this kind of applications.

Different control schemes were demonstrated in a hierarchical structure, where the upper level focused on optimising the operation according to variable electricity prices, while the lower level ensured robustness and safety of the operation.

Although work remains to be done to achieve a 24/7 optimal and reliable operation, this project demonstrated the feasibility of heat-pump-based boosting of supply temperature from a low temperature source to supply local district-heated areas in an energy flexible manner.

7 References

[1] Johra H., “Overview of the Coefficient of Performance (COP) for conventional vapour-compression heat pumps in buildings”, 2022, Aalborg University, technical report, https://doi.org/10.54337/aau459284067

[2] Grabo, M., Acar, E., & Kenig, E. Y. (2021). Modeling and improvement of a packed bed latent heat storage filled with non-spherical encapsulated PCM-Elements. Renewable Energy, 173, 1087-1097, https://doi.org/10.1016/j.renene.2021.04.022